Clim Dyn (2014) 42:2921–2929
DOI 10.1007/s00382-013-1748-2

Temperature projection in a tropical city using remote sensing and dynamic modeling

Janet Nichol · To Pui Hang · Edward Ng

Received: 24 January 2013 / Accepted: 13 March 2013 / Published online: 7 April 2013

Abstract Recent temperature projections for urban areas have only been able to reflect the expected change due to greenhouse-induced warming, with little attempt to predict urbanisation effects. This research examines temperature changes due to both global warming and urbanisation independently and applies them differentially to urban and rural areas over a sub-tropical city, Hong Kong. The effect of global warming on temperature is estimated by regressing IPCC data from eight Global Climate Models against the background temperature recorded at a rural climate station. Results suggest a mean background temperature increase of 0.67 °C by 2039. To model temperature changes for different degrees of urbanization, long-term temperature records along with a measureable urbanisation parameter, plot ratio surrounding different automatic weather stations (AWS) were used. Models representing daytime and nighttime respectively were developed, and a logarithmic relationship between the rate of temperature change and plot ratio (degree of urbanisation) is observed. Baseline air temperature patterns over Hong Kong for 2009 were derived from two ASTER thermal satellite images, for summer daytime and nighttime respectively. Dynamic raster modeling was employed to project temperatures to 2039 in 10-year intervals on a per-pixel basis according to the degree of urbanization predicted. Daytime and nighttime temperatures in the highly urbanized areas are expected to rise by ca. 2 °C by 2039. Validation by projecting observed temperature trends at AWS, gave low average RMS errors of 0.19 °C for daytime and 0.14 °C for nighttime, and suggests the reliability of the method.

Keywords Climate change · Remote sensing · Dynamic modeling · Temperature projection

1 Introduction

Global temperatures have increased at 0.13 °C per decade between 1956 and 2005 (IPCC 2007). Japan reported a 0.28 °C increase in annual temperature per decade between 1953 and 2000 (Matsumoto et al. 2003) while the United States reported a decadal increase of 0.19 °C from 1970 to 1997 (Knappenberger et al. 2001). In China, an average warming rate of 0.22 °C per decade was recorded by 710 weather stations across the whole country between 1951 and 2001 (Ren et al. 2004). As greenhouse-induced warming estimates involve the average temperature change over the world including places where urbanisation is absent, human factors, such as industrial expansion and land use changes (Kalnay and Cai 2003) may contribute additional temperature increases to urban areas. Thus under the combined effect of global warming and urbanisation, the rate of temperature increase in some urban areas may be faster than the global or country average (Leung et al. 2007). This needs further investigation in tropical and sub-tropical cities where high summer temperatures combine

Electronic supplementary material The online version of this article (doi:10.1007/s00382-013-1748-2) contains supplementary material, which is available to authorized users.

J. Nichol (✉) · T. P. Hang
Department of Land Surveying and Geo-Informatics, The Hong Kong Polytechnic University, Kowloon, Hong Kong
e-mail: lsjanet@polyu.edu.hk

E. Ng
Department of Architecture, The Chinese University of Hong Kong, New Territories, Hong Kong
e-mail: edwardng@cuhk.edu.hk

with often poor city design and increased affluence to multiply the use of air conditioning.

The effect of global warming on Hong Kong is indicated by the temperature change at Ta Kwu Ling (TKL) climate station in the northern New Territories as urban development is absent in this area (Lam 2006; Leung et al. 2007). Over the past 21 years, the annual mean temperature recorded at TKL has increased by 0.08 °C per decade (Fig. 1), and may be mainly attributed to global warming. Temperature trends in urban areas are usually characterized by data from the Hong Kong Observatory (HKO) Headquarters since it is situated in the dense urban core, in spite of its park-like setting. Here the annual mean temperature rose by only 0.16 °C per decade between 1948 and 2009 (Fig. 2), but by 0.28 °C per decade for the second half of the period from 1980 to 2009. Thus not only is the temperature rising faster than in rural areas, but alarmingly, the rate of increase itself is also increasing. This suggests that urbanisation is an additional factor in causing temperature rise, and if current trends are continued, temperatures could increase much faster in the future.

Since the urban infrastructure is known to alter the thermal environment creating an urban heat island (UHI) effect (Howard 1818), the dependence on urban features suggests

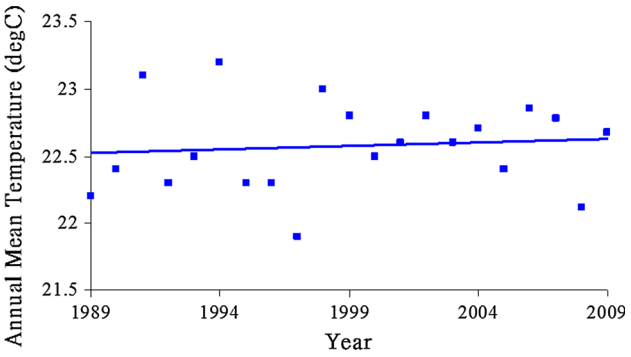

Fig. 1 Trend of annual mean temperature at Ta Kwu Ling from 1989–2009

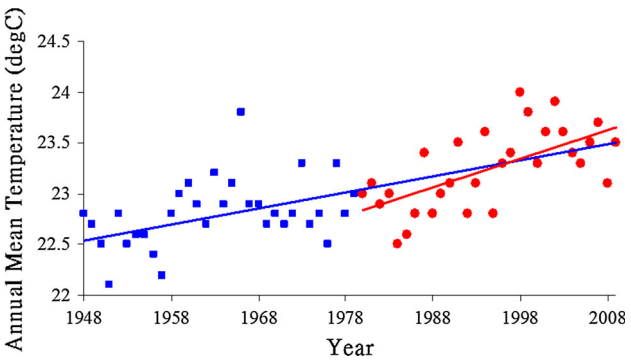

Fig. 2 Trend of annual mean temperature at HKO Headquarters from 1948–2009 (the *blue* and *red lines* represent the trend for the entire period and only the second half, respectively)

greater variability of temperatures over space in urban, than in rural areas. More spatially detailed temperature mapping and future temperature projections are therefore required, than can be provided by current climate models.

1.1 Objectives

The objective of this paper is to utilize state of the art remote sensing techniques, global climate models (GCMs), fixed station records and planning data to project summertime temperatures for Hong Kong over the next 30 years. The projection takes both greenhouse-induced warming as well as the effect of urbanisation into account. Daytime and nighttime temperature patterns are studied separately using satellite images taken for both day and night.

2 Temperature projection

2.1 Emission scenarios and uncertainty

The IPCC's Fourth Assessment Report (AR4) (IPCC 2007) stated the best estimate of global warming to be between 1.8 and 4.0 °C at the end of the twenty first century, relative to 1980–1999, with the wide range due to uncertainty of greenhouse gas (GHG) emissions. Future GHG emissions are assumed to follow one of six scenarios (Supplementary Fig. 1a), and for this project the A2 scenario was selected for the modeling because it lies mid-way between the highest and lowest scenarios for the relevant timeframe up to 2039 (Supplementary Fig. 1b). Timeframes beyond this are deemed unsuitable for this study, since urban parameters used in the modeling of urbanization effects are unavailable over a longer term.

2.2 Limitations of spatial resolution

The global climate models used in IPCC AR4 climate projections (IPCC 2007) are at coarse spatial resolution of over 100 km, and although those proposed for AR5 in 2014 (McCarthy et al. 2010; Oleson 2012) will consider urbanization effects at city-wide level, they will not recognize intra-urban heterogeneity, for projection of climatic change at intra-urban scale. Fine spatial resolution satellite imagery from thermal infra-red sensors such as Landsat ETM + and ASTER can provide a basis for more detailed modeling which allows urban scale effects to be considered, and many satellite-based urban climatic studies have been carried out [for a comprehensive review see Voogt and Oke (2003) and Weng (2009)]. Most previous research has only utilized satellite images for static climate modeling, but the development of advanced computing technology allows these images to be used for dynamic

modeling of processes whose spatial components change through time, as will be demonstrated in this paper.

2.3 Complexity of spatial dynamic modeling

Dynamic modeling can be defined as the modeling of processes which have spatial components that change through time (Karssenberg and De Jong 2005). The GCMs used in this project (Table 1) are types of spatial dynamic models because the input parameters vary over space and time (e.g. carbon dioxide concentration), but owing to their complexity, they are computationally and cost demanding. In this project, high resolution satellite imagery allows fine scale urban environment modeling with the aid of dynamic modeling software e.g. PCRaster (Utrecht University 2009), to integrate temporal data with satellite imagery. The temporal parameter i.e. rate of change is specified for each pixel, and an image at every time step is automatically generated using different input parameters at each step until the end of the study period (Van Beek and Van Asch 2004).

2.4 Temperature projection in Hong Kong

The Hong Kong Observatory (HKO) projected Hong Kong's annual mean temperature to 2100 by downscaling 15 IPCC AR4 models (Table 1) from regional to local level (Leung et al. 2007). To develop a model which relates the regional temperature to local temperature, they correlated the de-urbanised air temperature recorded at the HKO Headquarters with historical South China temperatures reanalyzed from the National Center for Environmental Prediction (NCEP). The projected data from global climate models (GCMs) were then fed into the regression relationship. The projections, which refer to the range of model ensemble for the six emission scenarios indicated that annual mean temperature in Hong Kong will rise by 3.0–6.0 °C by 2100, given no further urbanisation, and from 3.7 to 6.8 °C with a constant urbanisation rate as before. The urbanization effect was estimated from the urban heat island (UHI) magnitude (T(u − r)) from urban and rural climate stations over the last 100 years, as 0.08 °C per decade.

Compared with HKO's temperature projections for Hong Kong where a maximum of 6 °C or more is expected, those from other regions are relatively mild, with a maximum of 4 °C increase this century, predicted for Japan (Kurihara et al. 2005) and South America (Boulanger et al. 2006). As Hong Kong is the most densely built city in the world, many additional factors may contribute to the sharp increase in temperature, thus great uncertainty will remain unless these can be identified. Specifically, parameters representing urbanization are difficult to quantify for both past and future scenarios.

2.5 Modeling of urban parameters

Since the UHI is an effect of urbanization, not a causative factor, it cannot be used to parameterize a future prediction model. One parameter, the height-to-width ratio (H/W),

Table 1 Regression models used for downscaling, and the R^2 values, standard deviation (SD) of TKL observations for July to September, from 2000 to 2009, and the mean discrepancy between the predicted and observed temperatures for each model in the same period

Model	Regression Model y = model data x = TKL station data	R^2	n	Mean Discrepancy	Accept?
BCM2	$y = 0.9859x - 3.0664$	0.91	120	−0.14	Yes
CM3	$y = 0.9449x - 0.9997$	0.87	120	−0.32	No
MK3.0	$y = 1.2679x - 9.0459$	0.86	108	−0.36	No
*CM2.0	$y = 1.0848x - 4.0971$	0.85	108	−0.01	No
E20/Russell	$y = 0.8504x + 5.0524$	0.93	72	−0.12	Yes
CCSM3.0	$y = 1.2336x - 6.8555$	0.92	120	−0.20	Yes
PCM (V1)	$y = 1.1649x - 5.7879$	0.93	120	−0.14	Yes
HADCM3	$y = 1.2357x - 6.2108$	0.82	120	0.02	Yes
CGCM2.3.2a	$y = 1.0691x - 3.0463$	0.90	108	0.38	No
ECHO-G	$y = 1.1619x - 6.6416$	0.85	108	0.12	Yes
CM3.0	$y = 1.2961x - 10.74$	0.82	108	−0.41	No
ECHAM5	$y = 0.9362x + 0.7609$	0.80	108	−0.43	No
CM4 (V1)	$y = 1.757x - 21.04$	0.88	120	−0.10	Yes
*CGCM3.1	$y = 1.3493x - 11.095$	0.85	108	−0.28	No
MIROC (V3.2)	$y = 1.0233x - 0.8576$	0.89	108	−0.17	Yes

The n values denote the number of months available for each climate model

which is determined by the height and separation of buildings, has long been used to study the energy budget of the built environment (Oke 1982). Another parameter, the sky view factor (SVF) has also been found to be correlated with heat island intensity (Oke 1988). However, since neither the H/W ratio or SVF is used in Hong Kong for regulating city planning, a related parameter, the plot ratio is used in this research as the parameter defining the degree of urbanization. Plot ratio (PR), which also considers the density and height of buildings at a site is a widely accepted parameter in city planning and is defined as the gross floor area (GFA) of buildings divided by the site area, of each project site (Eq. 1).

$$PR = \frac{\sum a \times f}{A} \quad (1)$$

where a is the footprint area of a building, f is the number of floors and A is the corresponding site area.

3 Methods

3.1 Use of thermal satellite images for baseline air temperature mapping

Thermal satellite images from the ASTER satellite sensor on 22nd August 2009 daytime and 13th August 2008 nighttime, were geometrically and emissivity corrected and converted to air temperature by a procedure described in Nichol and To (2012). The emissivity correction (Nichol 2009) resulted in a pixel size of 10 m. The air temperatures were derived from a regression of the image surface temperatures against a series of air and surface temperature points collected in the field at the time of imaging, for which an R^2 of 0.74 and 0.82 were obtained for day and nighttime images respectively (Supplementary Figs. 2 and 3). When the image-derived air temperatures were validated against air temperatures at automatic weather stations, R^2 0.75 and 0.84 were obtained for day and night (Supplementary Figs. 4 and 5). As satellite images are often criticised for their temporal incompleteness, the two images were tested for their relevance to times and dates other than the time of imagery. The images were found to be representative of spatial patterns of air temperature over Hong Kong for 4 h during the day and 11 h during the night, on the imaging dates respectively (Supplementary Figs. 6 and 7). Furthermore, the pattern of temperature distribution on the nighttime image was able to represent 62 out of 69 dates during the summer months on which climatic conditions were similar to the imaging date, having hot weather and relatively clear skies for image collection. The daytime image was representative of 17 out of 76 dates (Nichol and To 2012). These results indicate the suitability of using satellite images for temperature modeling because they can accurately represent the spatial distribution of air temperature near ground level and are representative for extended time periods and a season rather than a single instant in time.

3.2 Projection for greenhouse-induced warming

Temperature was projected up to 2039 using a multi-model approach in order to improve the reliability and consistency of the results compared with a single model (Tebaldi and Knutti 2007). The simulation outputs of 15 global climate models, with the A2 emission scenario specified, were extracted from the Program for Climate Model Diagnosis and Inter-comparison (PCMDI) website, for the grid cell corresponding to Hong Kong. Due to the large grid sizes, the data are assumed be insensitive to temperature change at urban scale within Hong Kong. For downscaling to local scale, monthly temperatures recorded at the Ta Kwu Ling (TKL) station in Hong Kong were regressed against the GCM monthly outputs from January 2000, 2001 or 2004 depending on the earliest data in the GCMs, to December 2009. Since TKL is a typical rural area, any temperature change was assumed to be mainly due to global effects such as greenhouse warming.

Although high R^2 values ranging from 0.80 to 0.93 were obtained (Table 1), this does not necessarily imply accuracy of the predictions because there may be large offsets between observations and predictions. Therefore, since the interest of this project is the summer temperature, the monthly temperatures from July to September of each year, as well as those recorded at TKL, were averaged. Then the mean discrepancy between the observations and predictions of each GCM from 2000 to 2009 was calculated (Table 1).

The standard deviation of the seasonal temperatures at TKL over the same period was used as a threshold value to determine if the predictions were acceptable because this value reveals the normal year-to-year variation of the seasonal temperatures. Models whose prediction was greater than the SD of 0.3 at TKL were excluded as being unable to model the seasonal temperature in Hong Kong.

Although ten GCMs have discrepancies lower than the threshold value (SD) of 0.3 (Table 1), only eight were selected for temperature projection because the remaining two (marked *) actually predict a cooling trend, which contradicts the predictions of most GCMs, as well as trends observed over past decades (Figs. 1, 2).

For downscaling of temperature predictions from regional to local level, the monthly temperature outputs from 2010 to 2039 of the eight selected GCMs were fitted into the corresponding regression models (Table 1). The decadal summer temperatures predicted by each model

Table 2 Projected summer background temperature in the next 3 decades, from the monthly outputs from 2010 to 2039, of eight selected climate models using the regression equations for Ta Kwu Ling (rural) climate station listed in Table 1

Decade	Lower limit (°C)	Upper Limit (°C)	Ensemble mean (°C)	Projected temperature (°C)
2000–2009	N/A	N/A	N/A	27.8
2010–2019	0.05	0.53	0.24	28.0
2020–2029	−0.08	0.25	0.11	28.2
2030–2039	0.13	0.51	0.32	28.5
Total	0.10	1.29	0.67	N/A

The decadal summer temperatures predicted by each model were averaged to obtain an ensemble mean

were averaged to obtain an ensemble mean, and the upper and lower limits provided the maximum and minimum temperatures at the end of each decade (Table 2).

3.3 Projection of temperature due to urbanisation

The rates of temperature change at different urban locations would depend on the surrounding built environment since building materials create higher thermal load. The wide spatial spread of Hong Kong's AWS (Hong Kong Observatory 2013) provides a good opportunity to study temperature changes with respect to the surrounding environment. The hourly temperature data of eight AWS which have been established for at least 10 years and with continuous records since their establishment were obtained. Since no change in plot ratios had taken place at any of the sites since establishment, any temperature increases at these AWS should be attributed to territory-wide developments, which cause more heat to be retained by existing urban structures anywhere within the territory.

The hourly summertime (July to September) temperatures were grouped into daytime (10 a.m.–1 p.m.) and nighttime (6 p.m.–4 a.m.) temperatures respectively, periods during which temperature patterns remain constant [Nichol and To 2012 (Supplementary Figs. 6 and 7)], since temperature trends are expected to be different owing to different thermal processes during day and night (Voogt and Oke 2003). The yearly summer temperatures and the decadal temperature changes of each AWS for day and night respectively were computed (3). It is notable that the TKL weather station shows an increase of 0.08 and 0.07 °C per decade for day and night respectively, which is very similar to the overall background warming of 0.08 °C per decade as observed from the long term data for Hong Kong (Fig. 1). The temperature change solely due to urbanisation was obtained by subtracting background temperature increase at TKL from the total increases of the other stations.

3.4 Temperature change due to urbanisation, using plot ratios

The plot ratios of the street blocks where the eight selected AWS (Table 3) are situated were extracted and correlated with temperature changes at the corresponding sites. Street blocks are large irregular units used to group areas of similar built environment and thus their plot ratios are representative of a large region surrounding each AWS. Linear models were found inappropriate because no AWS are located in areas with very high plot ratios and the models would have given unreasonably fast temperature increase in such areas. A logarithmic function has been suggested to describe the relationship between urbanization and temperature (Karl et al. 1988), and between the H/W ratio and temperature (Oleson et al. 2008). As discussed in Sect. 3, plot ratio can be used to replace H/W. The logarithmic relation can be explained by the fact that air temperature is more closely related to horizontal surfaces ($r = 0.7$) than vertical surfaces ($r = 0.49$) (Nichol 1996). This implies that air temperature is more sensitive to density rather than height of buildings, though the latter

Table 3 Total and net temperature change per decade at the eight AWS

Stations	UCZ[a]	Year established	Total increase (Day)	Net increase (Day)	Total increase (Night)	Net increase (Night)
Cheung Chau	7	1992	0.03	−0.05	0.12	0.05
Ching Pak House	5	1987	0.92	0.84	0.75	0.68
Wong Chuk Hang	4	1989	0.41	0.33	0.29	0.22
King's Park	6	1992	0.27	0.19	0.37	0.3
Shatin	6	1984	0.2	0.12	0.2	0.13
Ta Kwu Ling	5	1985	0.08	0	0.07	0
Sai Kung	4	1993	0.46	0.38	0.5	0.43
Lau Fau Shan	5	1985	0.06	−0.02	0.09	0.02

[a] Urban Climate Zone, after Stewart and Oke 2009)

cannot be fully neglected. It can be assumed that the rate of temperature increase can be similar in areas with different plot ratios if there is no significant difference in the built densities, meaning that the plot ratio difference is a result of building height variations. In Hong Kong, most areas of high plot ratio are occupied by high rise buildings. It can be expected that the rate of temperature increase will slow down when the plot ratio has reached a certain level since temperature is less sensitive to the height of buildings. A logarithmic function can best model this relationship as it gives a slowing trend when the independent variable (i.e. plot ratio) increases.

3.5 Modeling future urban development

In this project, future plot ratios of sites were obtained from the Hong Kong government which announced the planned GFA/plot ratios for 44 projects, all of which are scheduled for increase in the next decade. The plot ratios of all street blocks over Hong Kong were input into the logarithmic equations (Eqs. 2, 3) in order to calculate the net temperature increase per decade. Pixels were assumed to have the same increase as the street block to which they belonged. These pixel-based incremental values were then added to the original temperatures of the pixel by decadal increments for the next 3 decades. The actual temperature increase was then obtained by adding the background warming rate (Table 2) to the net temperature increase. Therefore, in total 3 daytime and 3 nighttime future temperature maps were produced by dynamic modeling on a per-pixel basis, with the model parameters varied at each time step (i.e. decade).

3.6 Validation of temperature projections

For validation of the temperature projections the logarithmic models were used to back-project the outputs at 2039, to the year of establishment of the eight different AWS, and calculate the RMSE between the actual and projected change for the stations.

4 Results

The eight GCMs selected appear able to predict the monthly temperature in rural Hong Kong since 80 % to 93 % of the monthly temperature variations at the rural TKL station can be predicted by individual global climate models (Table 1). The correlations are all significant and much higher than obtained by Chan et al. (2010) who computed a low R^2 (−0.099 to 0.467) between annual temperatures in southern China and GCM outputs from the earliest available dates (i.e. January 2000, 2001 or 2004). The higher R^2 values for Hong Kong using monthly temperatures can be explained by the comparatively large inter-monthly temperature variation in Hong Kong within a year compared with relatively small (e.g. <1 °C) inter-annual temperature variations. The transfer of GCM outputs to the local level on a monthly basis (Maurer and Hidalgo 2008) appears more meaningful than annual.

The summer temperature at TKL is expected to increase by 0.24 °C in 2010–2019; 0.11 °C in 2020–2029 and 0.32 °C in 2030–2039 (Table 2). The relatively small increase of 0.11 °C in the third decade (2020–2029) may be explained by the influence of the emission reductions agreement later in the second decade (Copenhagen Accord 2009), which has been factored into the models. The total temperature increase in these three decades is estimated to be between 0.10 and 1.29 °C, with an ensemble mean of 0.67 °C.

For the temperature changes due to urbanization, a logarithmic relationship was observed in both the daytime and nighttime models (Eqs. 2, 3; Supplementary Figs. 8 and 9) (Sect. 3.4). Although urban development is frozen after the first decade due to lack of planning data beyond 2020, this relationship assumes that even if the plot ratio does not change, air temperature would still increase. This phenomenon can be explained by regional rather than local scale developments. In the past few decades, the whole of the Pearl River Delta (PRD) region has experienced rapid urbanization, with massive increase in population and buildings. The new developments would increase the heat storage capacity, with more long-wave radiation trapped by artificial materials (Oke and Maxwell 1975). Another source of increasing temperatures is the large number of factories in PRD releasing heat as a by-product of industry. As the temperature has been rising, more energy consumed by air conditioning, in turn releases more heat. This would create a large urban boundary layer (UBL) (Oke 1976), covering the whole PRD region including Hong Kong. The heat trapped in the UBL will diffuse across the UBL, and feed back into the UCL where urban structures in any area will reabsorb the heat. Thus temperatures would increase further in such areas even if there are no developments.

$$\text{Daytime: } y = 0.13 \ln x + 0.44 \quad (2)$$

$$\text{Nighttime: } y = 0.11 \ln x + 0.02 \quad (3)$$

where x = plot ratio, y = net temperature increase per decade.

The logarithmic regressions of the net temperature change per decade and plot ratio during the daytime and nighttime were $R^2 = 0.50$ and 0.56 respectively (Supplementary Figs. 8 and 9).

Validation of the outputs by back-projection, observed a mean RMSE between the actual and projected change for the stations, of 0.19 °C for daytime and 0.14 °C for nighttime.

5 Mapping the temperature projections

5.1 The daytime images

The summer daytime air temperature image (Fig. 3a) shows the inner urban areas of Kowloon Peninsula to be between 34.1 and 35.6 °C (light- and dark green areas). These are not the hottest areas due to the presence of building shadows, and thus reduced incoming radiation. Older urban districts with medium rise buildings (e.g. Kowloon City, as arrowed) are the warmest urban districts, with an additional 0.5 °C. The warmest areas correspond to large tracts of open ground (Supplementary Fig. 10) with little urban development corresponding to coastal reclaimed land in West Kowloon (orange area) (Supplementary Fig. 10). By 2039 (Fig. 3b) most urban areas will have a 2–3 °C increase in daytime air temperature, indicated by the original dark green areas changed to yellow. This indicates an average increase of temperature from currently around 35 °C to just less than 38 °C in 2039.

5.2 The nighttime images

At night, temperatures of the inner urban areas (29–31 °C) are significantly warmer than the surrounding non-built and vegetated areas (28.5–29 °C) and as in the daytime, older medium rise high density districts are the warmest (Fig. 4a). For example the purple areas in dense urban districts of Jordan (corresponding to the old Chinatown district) and Hung Hom (as arrowed), which are 0.7 °C hotter than their surroundings, can be regarded as the core of the UHI. Thus nighttime temperature hot spots are the densest built areas, whereas during the day the hottest areas are open spaces and low density built areas.

Over the next 3 decades nighttime temperatures in the centre of Kowloon are expected to show at least a 2 °C increase, reaching up to 32 °C (Fig. 4b, red and white areas). Open spaces should continue to be 1–2 °C cooler (the purple class) than the central urban area. The UHI will develop further to include more areas along the main shopping districts of Nathan Road and Tsim Sha Tsui (white areas) in the future. The intensity of the UHI should increase further as temperatures in urban areas will rise faster than in rural areas of lower plot ratios.

5.3 Mapping of bio-climatic parameters

The projected temperatures can be used to map the expected spatial distribution of bioclimatic variables such as thermal comfort levels (TS) as in Eq. (4), or wind requirements to achieve neutral sensation. The wind speed requirement is also calculated from Eq. 4 by setting the thermal sensation (TS) to 0, meaning neither a cold nor a hot condition and using image temperatures along with parameter values for a typical summer day and night situation in Hong Kong (Cheng et al. 2011). The maps show that nowhere in the urban areas except green space is thermally comfortable during a summer day, both at present and in the future. At night, most urban locations which are now ranked comfortable will become uncomfortable in 30 years' time (Supplementary Fig. 11). A minimum wind speed of 1.8–2.7 m/s and 0.3–0.8 m/s

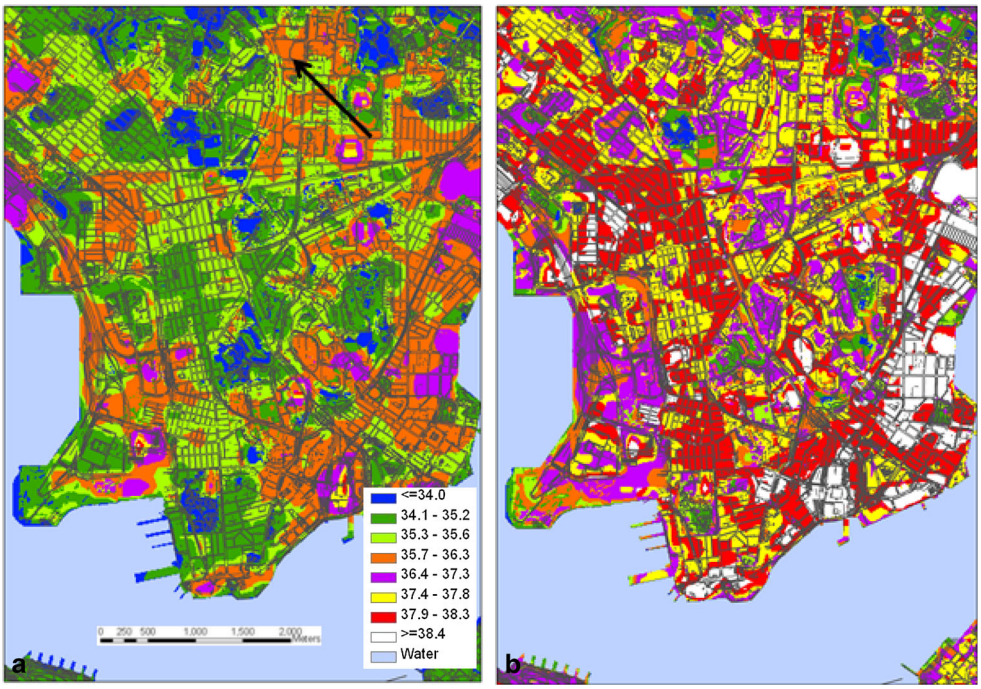

Fig. 3 **a** Daytime temperature map of Kowloon in 2009, **b** projected daytime temperature map of Kowloon in 2039

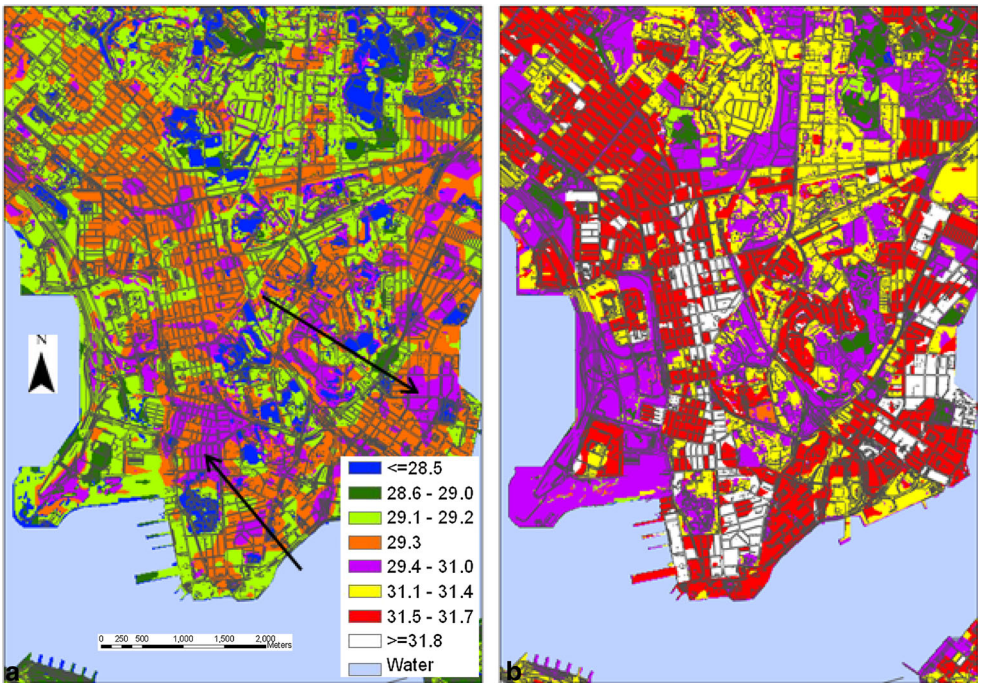

Fig. 4 **a** Nighttime temperature map of Kowloon in 2008, **b** projected nighttime temperature map of Kowloon in 2039

would be required to mitigate the daytime and nighttime heat in the urban areas respectively, to produce a neutral sensation (Supplementary Fig. 12). Since wind speeds in south China are expected to decrease as a result of global climate change (Zhao et al. 2011), such wind standards will become increasingly difficult to achieve (Cheng et al. 2011).

$$\mathrm{TS} = 0.1895 \times \mathrm{TA} - 0.7754 \times \mathrm{WS} + 0.0028 \times \mathrm{SR} + 0.1953 \times \mathrm{HR} - 8.23 \quad (4)$$

where TS is thermal sensation, TA is dry bulb air temperature (°C), WS is wind speed (m/s), SR is solar radiation (W/m^2) and HR is absolute humidity (g/kg).

6 Discussion

In the past few decades, temperature has demonstrated a rising trend in many countries and cities including Hong Kong. The rate of temperature increase at HKO near the centre of the urban area has been 0.28 °C per decade over the last 30 years while the rate of global warming was only 0.13 °C per decade over the last five decades. The faster temperature increase in Hong Kong can be explained by the combined effect of greenhouse-induced warming and urbanisation, which has been investigated here.

The projection models used in this project take both greenhouse warming and urbanisation into account, and are able to predict rates of temperature change in coming decades. Future temperature maps were produced dynamically at 10-year intervals using the iteration model (Sect. 3.5) and current satellite images. The daytime and nighttime temperatures in the highly urbanised areas (e.g. centre of Kowloon) are projected to rise by ca. 2 °C in 30 years' time. At the same time, temperature increases in rural areas in the absence of more urbanization are projected to be close to the greenhouse warming rate of 0.67 °C.

The main source of uncertainty in the predictions due to the urbanization effect lies in the fact that none of the eight AWS used for modeling temperature change due to urbanization are situated in an area with high plot ratios such as a high rise housing estate. Thus temperature trends are only estimated from changes in lower density areas, and a logarithmic trend has been assumed. This problem is difficult to rectify as climatic stations in Hong Kong, as in many cities, were originally located to monitor prevailing background weather conditions, with urban influences to be avoided. This also makes it unlikely that any change in plot ratios would have happened in the immediate surroundings of weather stations since their establishment. Therefore this study allows the modeling of temperature changes at AWS with reference to their current site plot ratios. This accounts for heat island effects and feedback from the urban boundary layer of the wider urbanized region of Hong Kong and neighbouring Pearl River Delta region which has experienced very rapid urban and industrial development over the last three decades.

The nighttime satellite image used for baseline mapping of air temperatures was more able to represent prevailing summertime temperatures over Hong Kong, than was the daytime image, as it was representative of air temperature distribution for 11 h surrounding the image time, and for

62 out of 69 (i.e. 90 %) of summer nights when weather conditions were similar i.e. no rainstorm or typhoon announced on that date. The longer period of validity at night is thought to be due to a more stable atmosphere with less convection and advection. The daytime image can be considered relevant for a shorter period during the day i.e. 9.30 a.m. to 1.30 p.m. and for about 25 % of summer days.

Validation of the projected temperatures, with a mean RMSE of 0.19 and 0.14 °C for 8 climate stations for day and night respectively suggests the models are reliable and that future increase will follow the predictions based on trends since the 1980s and 1990s to 2009 which is linked to plot ratios plus the background warming rate.

Acknowledgments The authors acknowledge Public Policy Research Grant 5006-PPR-09 from the Hong Kong government.

References

Boulanger JP, Segura EC, Martinez F (2006) Projection of future climate change conditions using IPCC simulations, neural networks and Bayesian statistics, Part 1. ClimDyn 27:233–259

Chan HS, Li TC, Yan WL (2010) Analysis of the modeling capability of IPCC AR4 climate models in the southern China region. Paper presented at the 24th Guangdong-Hong Kong-Macau seminar on meteorological science and technology, Shenzhen, China (in Chinese)

Cheng V, Ng E, Chan C, Givoni B (2011) Outdoor thermal comfort study in a sub-tropical climate. Int J Biometeorol. doi: 10.1007/s00484-010-0396-z

Copenhagen Accord (2009) http://www.denmark.dk/NR/rdonlyres/C41B62AB-4688-4ACE-BB7B-F6D2C8AAEC20/0/copenhagen_accord.pdf, Accessed 8th August 2011

Hong Kong Observatory (2013) Information on weather station. Accessed 7th March, 3013. http://www.hko.gov.hk/cis/annex/hkwxstn_e.htm

Howard L (1818) The Climate of London, vol 1. W. Philips, London

IPCC (2007) Climate Change (2007) Synthesis report. In: Pachauri RK, Reisinger A (eds), Contribution of working groups I, II and III to the fourth assessment report, IPCC, Geneva, p 104

Kalnay E, Cai M (2003) Impact of urbanization and land-use change on climate. Nature 423:528–531

Karl TR, Diaz HF, Kukla G (1988) Urbanization: its detection and effect in the United States climate record. J Clim 11:1099–1123

Karssenberg D, De Jong K (2005) Dynamic environmental modeling in GIS: 1. Modeling in three spatial dimensions. Int J Geogr Info Sci 19(5):559–579

Knappenberger PC, Michaels PJ, Davis RE (2001) Nature of observed temperature changes across the United States during the 20th century. Clim Res 17:45–53

Kurihara K, Ishihara K et al (2005) Projection of climate change over Japan due to global warming by high-resolution regional climate model in MRI. SOLA 1:97–100

Lam CY (2006) On climate changes brought about by urban living. Hong Kong Meteorol Soc Bull 16(1/2):15–20

Leung YK, Wu MC, Yeung KK, Leung WM (2007) Temperature projections in Hong Kong based on IPCC fourth assessment report. Hong Kong Meteorol Soc Bull 17:2

Matsumoto K, Ohta T, Irasawa M, Nakamura T (2003) Climate change and extension of the *Ginkgo biloba* growing season in Japan. Glob Change Biol 9(11):1634–1642

Maurer EP, Hidalgo HG (2008) Utility of daily vs. monthly large-scale climate data: an intercomparison of two statistical down-scaling methods. Hydrol Earth Syst Sci 12:551–563

McCarthy MP, Best MJ, Betts RA (2010) Climate change in cities due to global warming and urban effects. Geophys Res Lett 37:L09705. doi:10.1029/2010GL042845

Nichol JE (1996) High-resolution surface temperature patterns related to urban morphology in a topical city: a satellite-based study. J Appl Meteorol 35:135–146

Nichol JE (2009) An emissivity modulation method for spatial enhancement of thermal satellite images in urban heat island analysis. Photogramm Eng Remote Sens 75(5):547–556

Nichol JE, To PH (2012) Temporal characteristics of thermal satellite images for urban heat stress and heat island mapping. ISPRS J Photogramm 74:153–162

Oke TR (1976) The distinction between canopy and boundary-layer heat islands. Atmosphere 14:268–277

Oke TR (1982) The energetic basis of the urban heat island. Q J R Meteorol Soc 108:1–24

Oke TR (1988) Street design and urban canopy layer climate. Energy Build 11:103–113

Oke TR, Maxwell GB (1975) Urban heat island dynamics in Montreal and Vancouver. Atmos Environ 9:191–200

Oleson KW (2012) Contrasts between urban and rural climate in CCSM4 CMIP5 climate change scenarios. J Clim 25:1390–1412. doi:10.1175/JCLI-D-11-00098.1

Oleson KW, Bonan GB, Feddema J, Vertenstein M (2008) An urban parameterization for a global climate change model, Part II. J Appl Meteorol Climatol 47:1067–1076

Ren G, Xu M et al (2004) Climate change of the past 100 years in China. China Climate Change Info-Net. http://www.ccchina.gov.cn/en/NewsInfo.asp?NewsId=5439. Accessed Aug 20 2010

Stewart I, Oke TR (2009) A new classification system for urban climate sites. Bull Am Meteorol Soc 90:922–923

Tebaldi C, Knutti R (2007) The use of the multi-model ensemble in probabilistic climate projections. Philos Trans R Soc 365: 2053–2075

Utrecht University (2009) PCRaster Homepage. Accessed August 20, 2010, from http://pcraster.geo.uu.nl

Van Beek LPH, Van Asch THWJ (2004) Regional assessment of the effects of land-use change on landslide hazard by means of physically based modeling. Nat Hazards 31:289–304

Voogt JA, Oke TR (2003) Thermal remote sensing of urban climates. Remote Sens Environ 86:370–384

Weng Q (2009) Thermal infrared remote sensing for urban climate and environmental studies: methods, applications, and trends. ISPRS J Photogramm 64:335–344

Zhao Z, Luo Y, Jiang Y (2011) Is global strong wind declining? Adv Clim Change Res 2:225–228